Applied Catalysis B: Environmental 99 (2010) 156–162

Contents lists available at ScienceDirect

Applied Catalysis B: Environmental

journal homepage: www.elsevier.com/locate/apcatb

Origination of N_2O from NO reduction by NH_3 over β-MnO_2 and α-Mn_2O_3

Xingfu Tang[a,b], Junhua Li[b], Liang Sun[a,c], Jiming Hao[b,*]

[a] Department of Environmental Science and Engineering, Fudan University, Shanghai 200433, China
[b] Department of Environmental Science and Engineering, Tsinghua University, Beijing 100084, China
[c] College of Chemical Engineering, Huaqiao University, Xiamen 361021, China

ARTICLE INFO

Article history:
Received 15 March 2010
Received in revised form 12 May 2010
Accepted 7 June 2010
Available online 11 June 2010

Keywords:
Manganese oxides
Selective catalytic reduction
Nitric oxide
Ammonia activation
Nitrous oxide

ABSTRACT

Selective catalytic reduction (SCR) of NO with NH_3 was studied on β-MnO_2 and α-Mn_2O_3 catalysts at 150 °C and the formation of N_2O from SCR was mainly investigated. The activity evaluation showed that the rates of both NO conversion and N_2O formation per unit surface area on β-MnO_2 were much higher than the corresponding values on α-Mn_2O_3, while two catalysts gave same generated rate of N_2. Transient reactions of NO with NH_3 showed that N_2O predominantly originated from direct reaction of NO and NH_3 via an Eley–Rideal mechanism. β-MnO_2 gave higher generated rate of N_2O in transient reaction of NH_3 and more desorption amount of N_2O in temperature-programmed desorption of NH_3 than α-Mn_2O_3. The results of temperature-programmed reduction of H_2 exhibited that oxygen species on β-MnO_2 are more active than α-Mn_2O_3. Therefore, β-MnO_2 had higher selectivity to N_2O in SCR reaction than α-Mn_2O_3, predominantly resulting from higher activated capability to NH_3, and β-MnO_2 can cleave more N–H bonds in NH_3 molecules to give more adsorbed nitrogen atom species, which reacted with gaseous NO to form more N_2O.

1. Introduction

Nitrogen oxides (NO_x, $x = 1$ or 2) are the major air pollutants, which can cause adverse effects on the environment such as urban smog, acid rain and ozone depletion [1,2]. The SCR reaction of NO_x by NH_3 has proven to be the most efficient technology to treat stack of NO_x gases from stationary source. The general reaction occurs according to the following reaction (Eq. (1)).

$$4NO + 4NH_3 + O_2 \rightarrow 4N_2 + 6H_2O \quad (1)$$

Many transitional metal oxide catalysts have been proven to be active for SCR reaction, and commercially the V_2O_5/TiO_2 catalysts promoted with WO_3 or MoO_3 have been applied in the fields [3]. These catalysts are efficient at relatively high operating temperatures (300–400 °C) [4], which make it necessary to locate SCR unit upstream of electrostatic precipitator. Despite low sensitivity to SO_2 poisoning, the catalysts are still subjected to de-activity by high concentrations of SO_2 and ashes in the flue gas. Alternative is to locate the SCR unit downstream of the de-sulfurizer and electrostatic precipitator. However, the temperature of the flue gas at this location is lower than 150 °C, which makes it impracticable to apply the commercial V_2O_5/TiO_2 catalysts. Therefore, to develop inexpensive highly active catalysts for the SCR system at low temperatures is of importance.

Great efforts have been recently made to develop efficient catalysts for low-temperature SCR of NO by NH_3, and manganese oxide-based catalysts are among the most active catalysts. For instance, MnO_x/TiO_2 catalysts showed the best catalytic activity in SCR reactions among the first row transition metal oxides supported on TiO_2 at 120 °C [4]. Qi et al. [5] found that MnO_x–CeO_2 catalysts were several times more active than other catalysts reported in the literatures at temperatures below 150 °C. Yie and co-workers [6] investigated the pure manganese oxide catalysts prepared by precipitation method and found that higher oxidation state of manganese species was favorable for NO reduction by NH_3. Singoredjo et al. [7] studied extensively manganese oxides supported on alumina, and found that MnO_2/Al_2O_3 exhibited higher NO reduction activity than Mn_2O_3/Al_2O_3 per unit surface area at the same reaction condition. Subsequently, they studied the SCR reaction on a series of pure manganese oxides at low temperatures, and reported that both SCR activity and selectivity to N_2 were governed by average oxidation state of manganese, the degree of crystallinity and specific surface area [8]. Among them, MnO_2 exhibited higher catalytic activity and Mn_2O_3 exhibited higher selectivity to N_2. A generated rate of N_2O on MnO_2 is much higher than Mn_2O_3 at 150 °C based on equal total surface areas.

Environmentally, N_2O is a strong greenhouse gas, which can be concomitantly generated with N_2 in SCR of NO by NH_3 on some catalysts. At low temperatures, N_2O can originate from four overall reactions (Eqs. (2)–(5)) as follows:

$$3NO \rightarrow N_2O + NO_2 \quad (2)$$

* Corresponding author. Tel.: +86 10 62782195; fax: +86 10 62773650.
E-mail address: hjm-den@tsinghua.edu.cn (J. Hao).

0926-3373/$ – see front matter © 2010 Elsevier B.V. All rights reserved.
doi:10.1016/j.apcatb.2010.06.012

$$2NH_3 + 2O_2 \rightarrow N_2O + 3H_2O \quad (3)$$

$$4NO + 4NH_3 + 3O_2 \rightarrow 4N_2O + 6H_2O \quad (4)$$

$$4NO_2 + 4NH_3 + O_2 \rightarrow 4N_2O + 6H_2O \quad (5)$$

N_2O can result from the disproportionation reaction of NO (Eq. (2)) on the surface of the catalysts [9]. Besides this, Yamashita and Vannice [10] also reported that N_2O was formed via the reaction of NO with coordinatively unsaturated sites of Mn_2O_3 and Mn_3O_4 at low temperatures. N_2O is also formed from direct oxidation of NH_3 in the presence of O_2 (Eq. (3)) [11,12]. N_2O can derive from direct reaction of NO with adsorbed NH_3 (Eq. (4))[7,8], or from direct reaction of NO_2 with adsorbed NH_3 (Eq. (5)) [9,13,14].

The objective of this paper is to investigate the N_2O origination from SCR of NO by NH_3 at 150 °C over manganese oxide catalysts. Transition reactions of NH_3 and temperature-programmed desorption of NH_3 (NH_3-TPD) together with various characterization measurements such as X-ray photoelectron spectra (XPS), temperature-programmed reduction by H_2 (H_2-TPR) and pyridine adsorption infrared (Py-IR) spectra were conducted in order to find out the mechanism of N_2O formation.

2. Experimental

2.1. Catalyst preparation

β-MnO_2 and α-Mn_2O_3 catalysts were prepared by a redox hydrothermal method. A solid mixture composed of $MnSO_4{\cdot}H_2O$ (2.9140 g) and $(NH_4)_2S_2O_8$ (3.9344 g) was charged into a Teflon-lined autoclave (100 mL). The autoclave was filled with deionized water (75 mL), and then sealed and kept in an oven at 160 °C for 24 h and cooled to room temperature. The obtained black slurry was filtered, washed with deionized water and dried at 110 °C overnight. β-MnO_2 and α-Mn_2O_3 were obtained by calcining the sample in air at 400 °C for 4 h and 600 °C for 2 h, respectively.

2.2. Catalyst characterization

Morphologies of β-MnO_2 and α-Mn_2O_3 were investigated by scanning electron microscopy (SEM) (JEOL JSM-6700F), and detailed structures of the samples were examined with high resolution transmission electron microscopy (HRTEM) by a JEM 1010 electron microscope. X-ray powder diffraction (XRD) patterns were recorded with a D/Max-2500 powder diffractometer using nickel-filtered Cu Kα (λ = 0.15418 nm) radiation. Nitrogen adsorption–desorption isotherms of the samples were obtained at −196 °C using an AUTOSORB-1 instrument. The specific surface area was determined by using linear portion of Brunauer–Emmett–Teller (BET) model. H_2-TPR of the samples was carried out using a ChemiSorb 2720 adsorption instrument. The sample was reduced in stream of 10.0% H_2/Ar (50 mL/min) at a ramp rate of 10 °C/min. XPS were recorded at 25 °C on a PHI15300/ESCA spectrometer with an Al anode for Kα ($h\nu$ = 1484.6 eV) radiation. Charging effects were corrected by adjusting the binding energy (B.E.) of the C 1s peak to 284.8 eV. Py-IR was carried out on a BIO-RAD FTS3000 IR spectrometer. Self-supporting wafers of the samples (*ca.* 10 mg/cm^2) were made and loaded in an IR cell. The wafers were evacuated at 150 °C for 2 h for the record of the background spectrum. Then, the wafer was saturated with pyridine and evacuated at 150 °C for 2 h. Py-IR spectra were recorded at a spectra resolution of 4 cm^{-1} with subtraction of the sample background.

2.3. Catalytic evaluation

SCR of NO by NH_3 was performed in a fixed-bed quartz reactor (i.d. = 8 mm) under an atmospheric pressure at 150 °C. 200 mg catalyst (40–60 mesh) was charged for each run. The feed gas was composed of 680 ppm NO, 680 ppm NH_3, 3.0% O_2 (or 0% O_2) and balanced He, and the total flow rate was 300 mL/min, corresponding to a gas hourly space velocity (GHSV) of 90,000 mL/(g h). The concentrations of NO, NH_3, N_2O and NO_2 in the inlet and outlet gases were measured by an online FTIR analyzer (Gasmet DX4000, Finland), and the concentration of N_2 was detected by an online 7890A gas chromatograph (Agilent, USA) with a 5A molecular sieve column connected to a thermal conductivity detector. N_2O selectivity (S) was calculated by the following formula (Eq. (6)):

$$S(\%) = \frac{[N_2O]}{[N_2] + [N_2O]} \times 100 \quad (6)$$

where $[N_2O]$ and $[N_2]$ stand for the outlet N_2O and N_2 concentrations, respectively.

2.4. Transition reaction and NH_3-TPD

Transition reactions were carried out in a quartz tube reactor (i.d. = 8 mm) under an atmospheric pressure. The catalyst (200 mg, 40–60 mesh) was charged and pretreated in 3.0% O_2/N_2 at a total flow rate of 300 mL/min at 400 °C for 1 h, and cooled to 150 °C and purged with N_2, and then the catalyst was exposed to 680 ppm NO or/and 680 ppm NH_3, 3.0% O_2 (or 0% O_2), and balanced N_2 until adsorption saturation. NH_3-TPD was conducted after the above isothermal adsorption was finished. The catalyst with adsorption saturation of NH_3 was purged by pure N_2 to remove physically adsorbed species on the surface of the catalyst, and subsequently heated from 150 to 400 °C at 10 °C/min in a flowing N_2 (300 mL/min). For both transition reactions and NH_3-TPD, NO, NH_3, N_2O and NO_2 concentrations in the inlet and outlet gases were detected by an online FTIR analyzer (Gasmet DX4000, Finland) as a function of time or temperature, and desorption amount was calculated according to integral area of the corresponding desorption curve.

3. Results and discussion

3.1. Catalyst characterization

Fig. 1 shows the SEM images of two catalysts. Obviously, the samples display almost same morphology. An urchin-like microsphere can be seen in the SEM image of β-MnO_2, which is composed of numerous randomly oriented nanoflakes with widths of 100–150 nm and lengths of 400–800 nm, and the thickness of these nanoflakes is in a narrow range of *ca.* 30–40 nm. Particularly, α-Mn_2O_3 still maintains same morphologies as β-MnO_2 even though transformation of crystal structure occurred at 600 °C. Besides urchin-like microspheres, some nanoflakes and nanopinlikes can be also observed in the SEM images of α-Mn_2O_3. The chemical compositions of both β-MnO_2 and α-Mn_2O_3 have been determined by energy dispersive X-ray analysis (EDX). Manganese and oxygen elements are exclusively detected, from which average oxidation states (AOS) of manganese are calculated to be 3.9 for β-MnO_2 and 2.9 for α-Mn_2O_3, approaching to the corresponding theoretical values. The surface area of β-MnO_2 is 32.2 m^2/g, more than that (21.0 m^2/g) of α-Mn_2O_3.

Fig. 1 also shows the HRTEM images and fast Fourier transform (FFT) patterns of β-MnO_2 and α-Mn_2O_3. For β-MnO_2, the interplanar fringe spacings of 0.44 and 0.28 nm with a cross angle of 89° represent lattice spacings of the (1 0 0) and (0 0 1) planes, respectively, in crystal structure of β-MnO_2. Similarly, the fringe spacings of 0.31 and 0.27 nm with a cross angle of 77° are equal to interplanar distances of (1 2 2) and (2 2 −2) planes, respectively, in crystal structure of orthorhombic α-Mn_2O_3. Two corresponding FFT patterns are shown in the inset figures. The structures of β-MnO_2 and

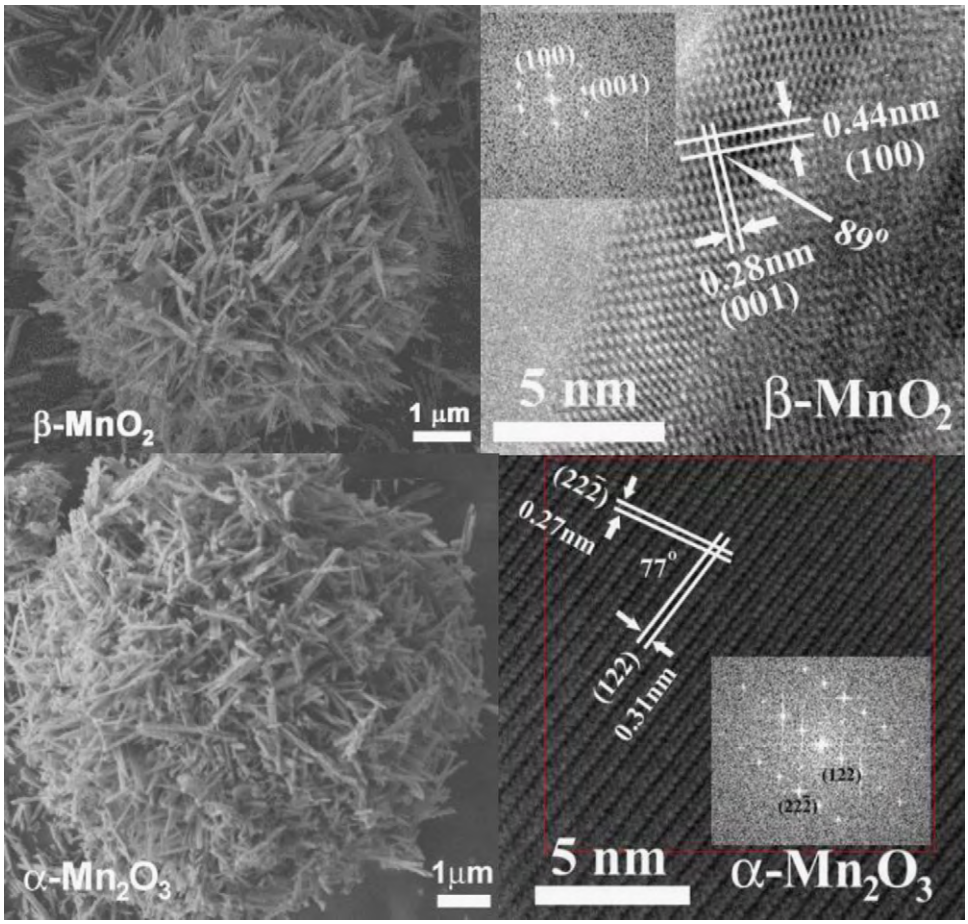

Fig. 1. SEM and TEM images of the catalysts.

α-Mn_2O_3 determined from the HRTEM images are consistent with the corresponding XRD data (Fig. S1, Supporting Information).

Fig. 2 shows the H_2-TPR profiles of the catalysts. The H_2-TPR profile of β-MnO_2 shows two reduction peaks, and a strong low temperature (LT) reduction peak is centered at 309 °C and a relatively weak high temperature (HT) one at 410 °C, and an area ratio of H_2 consumption of the LT peak to the HT one is *ca.* 2:1. The H_2-TPR profile of α-Mn_2O_3 also shows two reduction peaks at 353 and 450 °C and an area ratio of H_2 consumption of the LT peak to the HT one is *ca.* 1:2. Judged by the areas of the reduction peaks, the H_2 consumption of the LT peak of β-MnO_2 is as four times as the LT one of α-Mn_2O_3, whereas the H_2 consumptions of the HT peaks of two catalysts are almost equal. Consequently, the LT reduction peak represents reduction of MnO_2 or Mn_2O_3 to Mn_3O_4 and the HT one refers to further reduction of Mn_3O_4 to MnO [15,16]. The H_2 consumption of β-MnO_2 is 10.9 mmol/g, much more than that (6.8 mmol/g) of α-Mn_2O_3, from which AOS of manganese are calculated to be 3.9 for β-MnO_2 and 3.1 for α-Mn_2O_3, by assuming that MnO is a final reduction product [8]. The reduction temperature of β-MnO_2 is lower than that of α-Mn_2O_3. One can transfer horizontally the peaks of α-Mn_2O_3 to the low temperature region by 40 °C of shift. Interestingly, both positions and shapes of the peaks of α-Mn_2O_3 are identical to the corresponding ones of β-MnO_2 as shown in Fig. 2, and the similar findings have been observed in the H_2-TPR profiles of various manganese oxides prepared from the pyrolysis of the same precursor [8]. Generally, the same morphology of manganese oxides with different crystal structures can be maintained via the heat-treatment of the same manganese oxide precursor [17]. Therefore, the same curves in the H_2-TPR profiles of β-MnO_2 and α-Mn_2O_3 possibly are closely associated with their same morphologies. The result strongly suggests that Mn–O bonds of β-MnO_2 have much lower average energies than ones of α-Mn_2O_3, and the former was cleaved by H_2 molecule more easily.

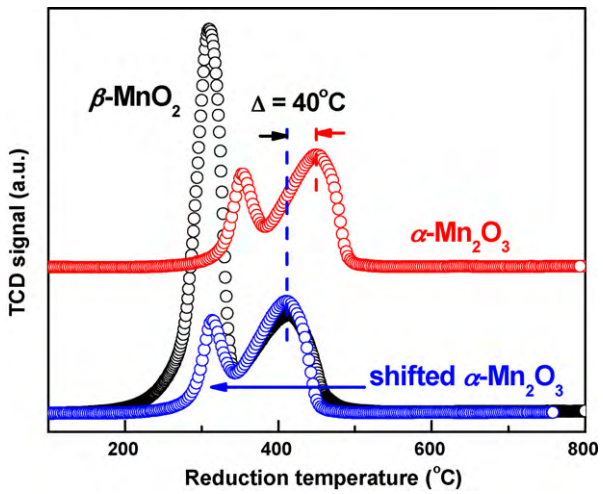

Fig. 2. H_2-TPR profiles of the catalysts.

Fig. 3 shows the O 1s XPS results of the catalysts. Two kinds of surface oxygen species could be distinguished in the O 1s XPS. Lower B.E. of 529.0–530.0 eV could be ascribed to oxygen ions (O_s) bound to metal cations in a coordinatively saturated environment [18], and higher B.E. of 531.0–532.0 eV might be assigned to surface

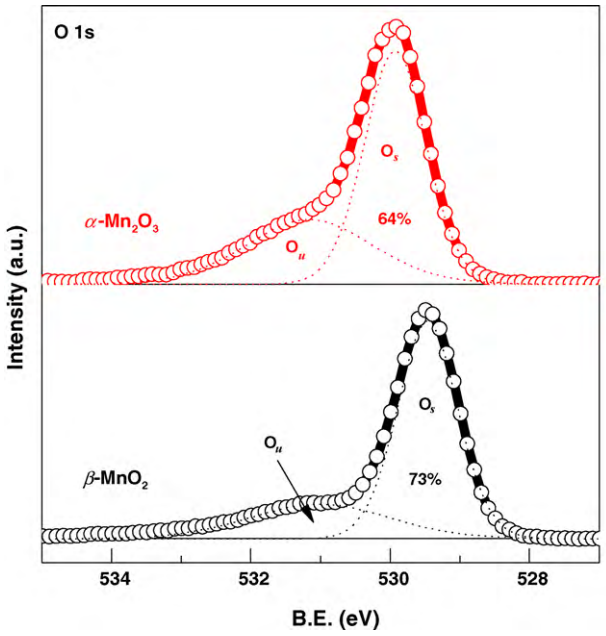

Fig. 3. O 1s XP spectra of the catalysts.

oxygen ions (O_u) bound to metal cations in a coordinatively unsaturated environment [18]. The ratio of $O_u/(O_s + O_u)$ on the surface of α-Mn_2O_3 is 36%, more than that (27%) of β-MnO_2, implying that α-Mn_2O_3 has more surface manganese cations in a coordinatively unsaturated environment (Mn_u).

The Py-IR spectra of β-MnO_2 and α-Mn_2O_3 are shown in Fig. 4. Two characteristic bands at *ca.* 1440 and 1550 cm^{-1} are frequently assigned to pyridine adsorption on Lewis acid sites and Brønsted acid sites, respectively. Clearly, a weak band at 1446 cm^{-1} for β-MnO_2 and an intense band at 1444 cm^{-1} for α-Mn_2O_3 indicate that α-Mn_2O_3 possesses much stronger Lewis acid sites than β-MnO_2, which is consistent with more Mn_u of α-Mn_2O_3, as evidenced by the XPS result. Moreover, a band at 1475 cm^{-1} can be observed for both cases, which have also been found in the Py-IR on the HY zeolites [19], and judged from their intensity, the band possibly results from the interaction between the adsorbed pyridine and manganese oxides. Thus, both β-MnO_2 and α-Mn_2O_3 show the absence of a band at *ca.* 1550 cm^{-1}, indicative of the lacks of strong Brønsted acid sites in both samples.

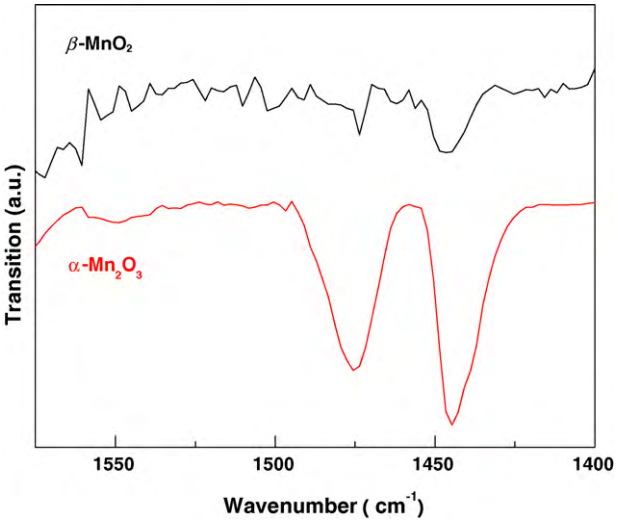

Fig. 4. Py-IR spectra of the catalysts.

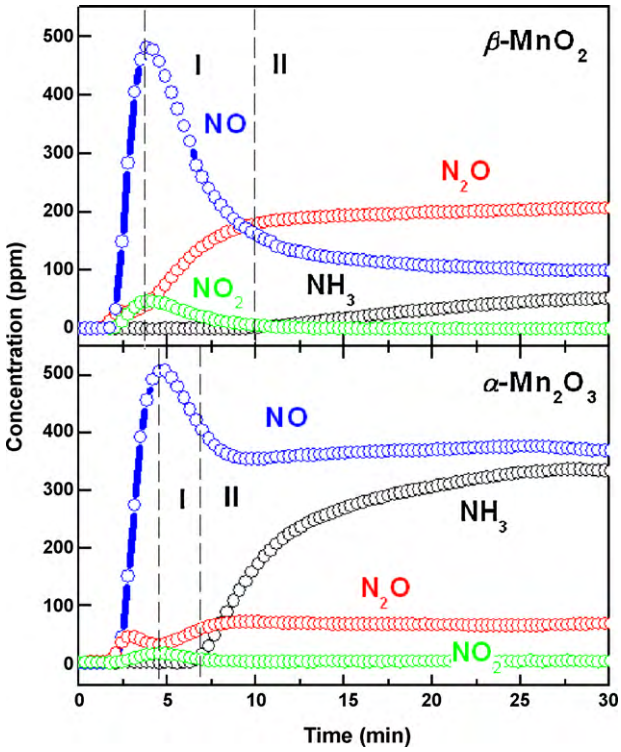

Fig. 5. Transition reactions of NH_3 + NO on the catalysts in the presence of O_2. Conditions: catalyst = 200 mg, NO = 680 ppm, NH_3 = 680 ppm, O_2 = 3.0%, and N_2 balance, gas rate = 300 mL/min, temperature = 150 °C.

3.2. Catalytic activity and selectivity

Fig. 5 shows the results of transition reactions of NH_3 + NO on the catalysts in the presence of O_2 at 150 °C. The adsorption capacity of α-Mn_2O_3 for NO is slightly stronger than that of β-MnO_2, whereas the adsorption capacity of NH_3 on the latter is much stronger than the former. The emissions of NO from both catalysts speedily increase up to a maximum and then decrease to a steady state. Detailed studies find that the decrease of NO concentration involves two stages: at the first stage (I) the NO concentration speedily decreases, and at the second stage (II) it slowly decreases to a steady state. Coincided with this process, NH_3 adsorption reached a saturated adsorption state on the catalysts at the first stage, and then the emitted concentration of NH_3 gradually increases and levels off at the second stage. The results elucidate that the decrease of gaseous NO concentration probably results from reaction of adsorbed N and NH_x (x = 1 or 2) species with gaseous NO through a typical Eley–Rideal (ER) mechanism [8,9,20], and the rates of this reactions occurred on β-MnO_2 are faster than that on α-Mn_2O_3 on the base of lower outlet concentrations of NO and NH_3 for the former.

NO reduction by NH_3 in the presence of O_2 was conducted on the catalysts at 150 °C, and the results are listed in Table 1. The conversions of NO and NH_3 on β-MnO_2 are 86.1% and 89.2%, respectively, almost twice as the corresponding values on α-Mn_2O_3. NH_3 conversions are almost equal to the corresponding NO conversions for both cases, suggesting that NO reacts in a 1:1 molar ratio with NH_3 in the reactions, in agreement with the previous results [7,8]. The yield of N_2 on β-MnO_2 is higher than that on α-Mn_2O_3. Remarkably, β-MnO_2 achieves 30.0% yield of N_2O, much higher than 8.8% of α-Mn_2O_3, and thus β-MnO_2 gives *ca.* 35% selectivity to N_2O,

Table 1
Conversion, yield and specific reaction rate (R_s) on β-MnO_2 and α-Mn_2O_3 in the SCR reactions in the presence of O_2[a].

Reactant/product	Conversion or yield (%)		R_s ($\times 10^{-9}$ mol/(s m^2))	
	β-MnO_2	α-Mn_2O_3	β-MnO_2	α-Mn_2O_3
NO	86.1	43.6	19.6	15.2
NH_3	89.2	44.8	20.2	15.6
N_2	56.0	35.0	13.1	12.5
N_2O	30.0	8.8	6.8	3.1

[a] Conditions: catalyst = 200 mg, NO = 680 ppm, NH_3 = 680 ppm, O_2 = 3.0%, and He balance, gas rate = 300 mL/min, and temperature = 150 °C.

higher than 20% of α-Mn_2O_3. Specific reaction rates (R_s) in terms of converted or generated amounts per unit of surface area and per second are also listed in Table 1. The R_s of NO and NH_3 of β-MnO_2 are higher than the corresponding values of α-Mn_2O_3, and two catalysts give almost equal R_s of N_2. Noticeably, the R_s of N_2O of β-MnO_2 is 6.8×10^{-9} mol/(s m^2), more than two times of 3.1×10^{-9} mol/(s m^2) of α-Mn_2O_3.

The SCR of NO by NH_3 was also conducted in the absence of O_2 at the same temperature and the results are listed in Table S1. The reaction rates of NO and NH_3 in the absence of O_2 are much slower than the corresponding values in the presence of O_2, indicative of great enhancement of O_2 in the reaction of NO by NH_3. Specially, conversions of NO and NH_3 on α-Mn_2O_3 are less than 6%, while conversions of NO and NH_3 on β-MnO_2 are more than 20%, suggesting that lattice oxygen from Mn–O bond with lower energy on the surface of β-MnO_2 can participate into the SCR reaction easily, and that oxygen "tightly" bound to manganese (higher Mn–O bond energy) on α-Mn_2O_3 seems difficult for this reaction. Therefore, the Mn–O bond energies of manganese oxides have an important role in the SCR reaction, in good agreement with the previous studies [7,8,21].

3.3. Origination of N_2O

In the SCR reactions, two nitrogen atoms of N_2O can originate from two same molecules such as NO or NH_3 alone. Compared the transition reactions in Fig. 5 with Figs. S2 and S3, one can find that the peaks of the N_2O curves almost appear at the same adsorption time (*ca.* 2.5 min) regardless of the presence of NH_3 and/or O_2, indicating that disproportionation reaction (Eq. (2)) of NO simultaneously occurs with the SCR reaction (Eq. (1)). The time (*ca.* 1.8 min) required for the generation of NO_2 from the SCR reaction in Fig. 5 is shorter than that (more than 2.3 min) of N_2O from direct oxidation of NH_3 in the forthcoming Fig. 6. Thus, N_2O under the SCR reaction conditions possibly does not derive from direct oxidation reaction (Eq. (3)) of NH_3 due to NO_2 being a more efficient oxidant than O_2 or NO [22].

Two nitrogen atoms of N_2O can also come from two different molecules: one from NO and another from NH_3. The decreases of both NO and NO_2 concentrations are coincident with the increase of N_2O concentrations in Fig. 5, implying that (i) reactions of gaseous NO with adsorbed NH_x and N species via the ER mechanisms following the reactions (Eqs. (1) and (4)) probably take place to give N_2 and N_2O, respectively [9,13,14], and (ii) gaseous NO_2 reacts with adsorbed NH_3 in the presence of NO to give N_2 following the Fast SCR reaction rather than does as the reaction (Eq. (5)) since the former is much faster than that of the latter [23]. The postulation has been substantiated by the isotopic labeling experiments on manganese oxides at 150 °C performed by Singoredjo et al. [7]. The results of SCR of NO by $^{15}NH_3$ showed that ^{15}NNO was formed in appreciable amounts, whereas $^{15}N_2O$ was not detected under the same SCR reaction conditions.

In the current SCR reaction, N_2O mainly originates from two reactions (Eqs. (2) and (4)) on the base of the above discussion. Suppose the generated NO_2 could be completely converted to N_2 [23], the R_s of ½N_2O from the reaction (Eq. (2)) on β-MnO_2 is 0.6×10^{-9} mol/(s m^2), approaching to 0.7×10^{-9} mol/(s m^2) on α-Mn_2O_3 as listed in Table S2. Calculated from Table 1, the total R_s of ½N_2O in the SCR reactions are 13.6 and 6.2×10^{-9} mol/(s m^2) for β-MnO_2 and α-Mn_2O_3, respectively. Thus, N_2O from direct reaction of NO with NH_3 can be contributed to *ca.* 95.6% and 88.7% of total amounts of N_2O in the SCR reactions for β-MnO_2 and α-Mn_2O_3, respectively. Therefore, N_2O predominantly originates from direct reaction of NO with NH_3 for both cases under the SCR conditions.

3.4. Possible formation mechanism of N_2O

Fig. 6 gives transition reaction curves of $NH_3 + O_2$ on the catalysts. Both catalysts give similar adsorption curves of NH_3. The time required for saturated adsorption of NH_3 is 4–5 min, much longer than that (*ca.* 2.0 min) of NO adsorption (Fig. S3). The result implies that the catalysts have stronger adsorption capability for NH_3 than NO. The R_s of ½N_2O on β-MnO_2 is 1.4×10^{-9} mol/(s m^2), much more than 0.5×10^{-9} mol/(s m^2) on α-Mn_2O_3 calculated from Fig. 6, and amounts of both NO and NO_2 can be negligible for both cases. The activation of NH_3 has been proven to proceed via successive stripping of hydrogen atoms from NH_3 molecules by oxygen species [24]. For oxidation reaction of NH_3 on manganese-based catalysts, to a great extent the oxidation state of manganese governs selectivity to N_2O, and higher oxidation state of manganese frequently results in higher selectivity to N_2O [24,25]. Another convincing and essential evidence originates from the results reported by Il'Chenko and Golodets [11,12]. They had investigated oxidation of NH_3 over MnO_2 amongst other transition metal oxides, and found that lower surface oxygen bond energy results in greater amounts of deep oxidation product (N_2O). The same mechanism is probably accepted for interpretation of the current results.

The NH_3-TPD profiles of the catalysts are shown in Fig. 7. Two catalysts give similar broad NH_3 desorption curves in a temperature window of 180–320 °C with a maximum at 240 °C. In a slightly higher temperature region, both N_2O and NO are desorbed, which generated from reaction of adsorbed NH_3 with surface oxygen species of the catalysts. Indeed, in oxidation of NH_3 by O_2 on MnO_2, probably, both N_2 and N_2O are simultaneously produced in the

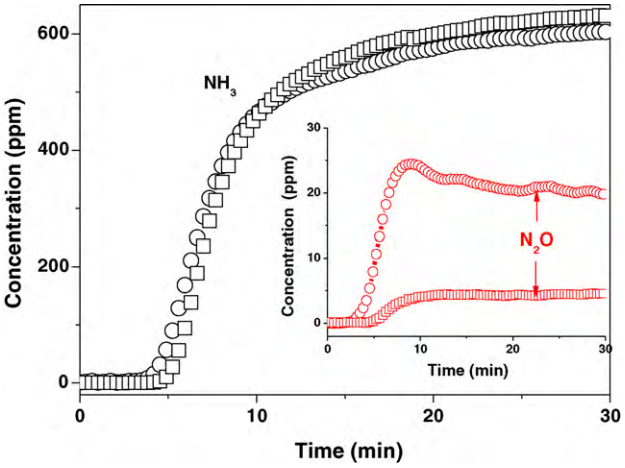

Fig. 6. Transition reactions of $NH_3 + O_2$ on β-MnO_2 (○) and α-Mn_2O_3 (□). Conditions: catalyst = 200 mg, NH_3 = 680 ppm, O_2 = 3.0%, and N_2 balance, gas rate = 300 mL/min, and temperature = 150 °C.

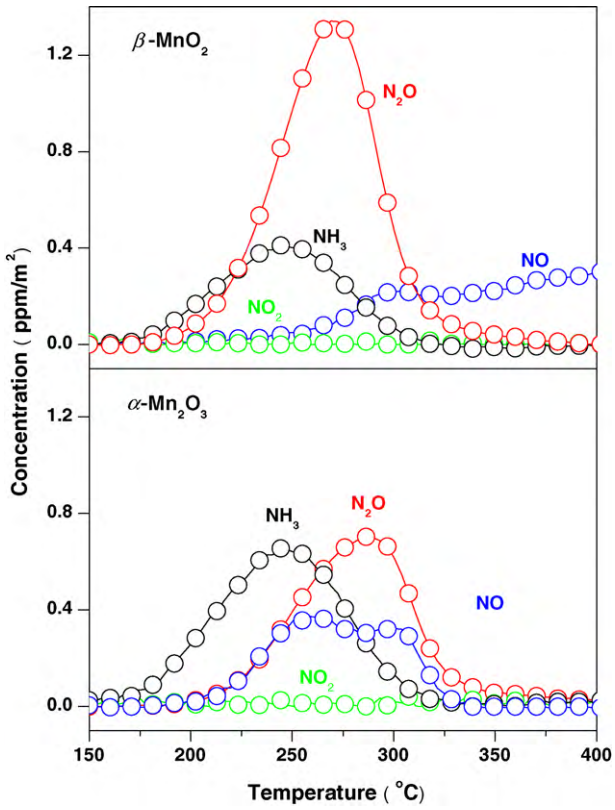

Fig. 7. NH_3-TPD profiles of the catalysts. Conditions: catalyst = 200 mg, gas rate of N_2 = 300 mL/min, and heated rate = 10 °C/min.

NH_3 desorption process over the current catalysts according to the reports of Il'Chenko and Golodets [11,12].

The desorption amounts of NH_3, N_2O and NO per unit of surface area of manganese oxides are listed in Table 2, which are calculated by integration of the areas under the NH_3-TPD curves in a temperature range of 150–400 °C from Fig. 7. The desorption amounts of NH_3 from β-MnO_2 are 0.2 μmol/m^2, half of the corresponding value of 0.4 μmol/m^2 from α-Mn_2O_3, strongly suggesting that gaseous NH_3 molecules were desorbed from Mn_u, where NH_3 coordinately adsorbed through coordination bond of Mn–NH_3 without cleavage of N–H bonds [9]. This result is in line with stronger Lewis acid of α-Mn_2O_3 as confirmed by Py-IR spectra. Noticeably, the desorption amount of ½N_2O from β-MnO_2 is 1.1 μmol/m^2, much more than 0.7 μmol/m^2 from α-Mn_2O_3. The results indicate that there are different active sites on the catalysts for adsorption and activation of NH_3. Moreover, the total amount of ½N_2O + NO from β-MnO_2 is 1.3 μmol/m^2 more than 1.2 μmol/m^2 from α-Mn_2O_3, though desorption amounts (0.2 μmol/m^2) of NO from β-MnO_2 is less than the corresponding value (0.5 μmol/m^2) from α-Mn_2O_3, and amounts of NO_2 can be negligible for both cases. This implies that other active sites for NH_3 adsorption are surface oxygen species, where NH_3 adsorbed dissociatively on these oxygen species by abstraction of all hydrogen atoms to form adsorbed nitrogen atom species, which are responsible for the generations of N_2, N_2O and NO [26].

Table 2
NH_3-TPD results from 150 to 400 °C at a heated rate of 10 °C/min after saturation adsorption of NH_3 at 150 °C in the presence of O_2 (unit: μmol/m^2).

Sample	NH_3	½N_2O	NO	½N_2O + NO
β-MnO_2	0.2	1.1	0.2	1.3
α-Mn_2O_3	0.4	0.7	0.5	1.2

Although there are some disagreements on the formation mechanism of N_2O in SCR reaction of NO by NH_3 depending on the nature of the catalysts, the ER mechanism via reaction of adsorbed NH_3 with gaseous NO has been supported by some researchers [5,20,24,27]. Janssen et al. [28,29] studied the mechanism of the reaction of NO, NH_3 and O_2 on Vanadia catalysts using isotopic ^{18}O and $^{15}NH_3$, and the main results included three aspects: (i) the amount of ^{15}NNO is much more than other nitrous oxides ($^{15}NN^{18}O$, $N_2{}^{18}O$ or N_2O), (ii) the concentration of H_2O is much higher than that of $H_2{}^{18}O$, and (iii) the reaction of O_2 is faster than reaction of NO with the catalyst. These results suggested that the oxygen remains bonded to the nitrogen in NO molecule to give ^{15}NNO, implying that the reaction of adsorbed ^{15}N atom with gaseous NO gives ^{15}NNO, and that the reaction of NO with adsorbed $^{15}NH_x$ species to give H_2O and ^{15}NN. Meanwhile, Kapteijn et al. [8] studied the interaction of NO, NH_3 and O_2 on manganese oxide, and proposed a model that NH_3 was successively dehydrogenated by surface oxygen to the N and NH_x intermediates, and then reacted with gaseous NO via the ER mechanism to the products. They proposed that the NH_2 intermediate could react with gaseous NO to form N_2, while NH or N species could react with NO to only give N_2O. According to the above results, the kind of the NH_x or N intermediates plays a crucial role in determining selectivity to N_2O in the SCR reaction.

On the base of the experimental data and the above discussion, the selectivity to N_2O predominantly derives from activated capabilities to NH_3 on the manganese oxide catalysts. One nitrogen atom of N_2O originates from NO and another from NH_3 (Eq. (4)), and three N–H bonds must be cleaved by surface oxygen species of the manganese oxides to form N_2O. Thus, the active oxygen species of the manganese oxides (low Mn–O bond energy) facilitate the cleavage of three N–H bonds of NH_3 molecule to give adsorbed nitrogen atom species, which lead to the formation of N_2O. The H_2-TPR data show that surface oxygen species on β-MnO_2 are more active than ones of α-Mn_2O_3, which exhibits higher abilities to activate the NH_3 molecules as shown in Figs. 5 and 6. The activation of NH_3 on β-MnO_2 should produce more adsorbed nitrogen atom species besides adsorbed NH_x, while the predominant intermediate species produced from NH_3 on α-Mn_2O_3 are NH_x. Compared with α-Mn_2O_3, β-MnO_2 with lower Mn–O bond energy can cleave more N–H bonds in NH_3 molecule to form more N species, which reacts with the gaseous NO via the ER mechanism to result in higher selectivity to N_2O. Therefore, higher selectivity to N_2O in the SCR reaction on β-MnO_2 essentially associated with lower Mn–O bond energy than α-Mn_2O_3. The results are helpful to develop new catalysts for NH_3-SCR of NO_x with high NO_x conversion but low selectivity to N_2O.

4. Conclusions

β-MnO_2 and α-Mn_2O_3 were prepared by the redox hydrothermal route and investigated in NO reduction by NH_3 at 150 °C. The catalytic evaluation showed that β-MnO_2 achieved higher conversion of NO, higher specific generated rate of N_2O and almost same specific generated rate of N_2 per unit surface area with respect to α-Mn_2O_3. Transient reactions of NO with NH_3 showed that N_2O predominantly originated from direct reaction of NO with NH_3 via an Eley–Rideal mechanism. The results of NH_3-TPD and transition reactions of NH_3 revealed that β-MnO_2 gave higher amounts of N_2O than α-Mn_2O_3 in both cases. The H_2-TPR analyses showed that β-MnO_2 has lower Mn–O bond energies than α-Mn_2O_3. These results demonstrated that β-MnO_2 possessed higher activated capability to NH_3 molecules and can cleave more N–H bonds in NH_3 molecules to give more adsorbed nitrogen atom species, which reacted with

gaseous NO to form more N_2O. Therefore, β-MnO_2 had higher selectivity to N_2O in SCR reaction than α-Mn_2O_3

Acknowledgements

This work was financially supported by Natural Science Foundation of China (20977018), Natural Science Foundation of Shanghai (09ZR1402500) and the National High-Tech Research and Development (863) Program of China (2007AA061802).

Appendix A. Supplementary data

Supplementary data associated with this article can be found, in the online version, at doi:10.1016/j.apcatb.2010.06.012.

References

[1] V.I. Pârvulescu, P. Grange, B. Delmon, Catal. Today 46 (1998) 233–316.
[2] H. Schneider, S. Tschudin, M. Schneider, A. Wokaun, A. Baiker, J. Catal. 147 (1994) 5–14.
[3] G. Busca, L. Lietti, G. Ramis, F. Berti, Appl. Catal. B: Environ. 18 (1998) 1–36.
[4] P.G. Smirniotis, D.A. Peña, B.S. Uphade, Angew. Chem. Int. Ed. 40 (2001) 2479–2482.
[5] G. Qi, R.T. Yang, R. Chang, Appl. Catal. B: Environ. 51 (2004) 93–106.
[6] M. Kang, E.D. Park, J.M. Kim, J.E. Yie, Appl. Catal. A: Gen. 327 (2007) 261–269.
[7] L. Singoredjo, R. Korver, F. Kapteijn, J. Moulijn, Appl. Catal. B: Environ. 1 (1992) 297–316.
[8] F. Kapteijn, L. Singoredjo, A. Andreini, J.A. Moulijn, Appl. Catal. B: Environ. 3 (1994) 173–189.
[9] S. Suárez, J.A. Martín, M. Yates, P. Avila, J. Blanco, J. Catal. 229 (2005) 227–236.
[10] T. Yamashita, A. Vannice, Appl. Catal. B: Environ. 13 (1997) 141–155.
[11] N.I. Il'Chenko, G.I. Golodets, J. Catal. 39 (1975) 57–72.
[12] N.I. Il'Chenko, G.I. Golodets, J. Catal. 39 (1975) 73–86.
[13] G. Madia, M. Koebel, M. Elsener, A. Wokaun, Ind. Eng. Chem. Res. 41 (2002) 4008–4015.
[14] C. Ciardelli, I. Nova, E. Tronconi, D. Chatterjee, B. Bandl-Konrad, M. Weibel, B. Krutzsch, Appl. Catal. B: Environ. 70 (2007) 80–90.
[15] E.R. Stobbe, B.A. de Boer, J.W. Geus, Catal. Today 47 (1999) 161–167.
[16] T. Chen, H.Y. Dou, X.L. Li, X.F. Tang, J.H. Li, J.M. Hao, Micropor. Mesopor. Mater. 122 (2009) 270–274.
[17] Z.H. Yang, Y.C. Zhang, W.X. Zhang, X. Wang, Y.T. Qian, X.G. Wen, S.H. Yang, J. Solid State Chem. 179 (2006) 679–684.
[18] F. Larachi, J. Pierre, A. Adnot, A. Bernis, Appl. Surf. Sci. 195 (2002) 236–250.
[19] A. Boréave, A. Auroux, C. Guimon, Micropor. Mater. 11 (1997) 275–291.
[20] W.S. Kijlstra, D.S. Brands, H.I. Smit, E.K. Poels, A. Bliek, J. Catal. 171 (1997) 219–230.
[21] G. Ramis, Y. Li, G. Busca, M. Turco, E. Kotur, R. Willey, J. Catal. 157 (1995) 523–535.
[22] M. Koebel, G. Madia, F. Raimondi, A. Wokaun, J. Catal. 209 (2002) 159–165.
[23] M. Koebel, M. Elsener, M. Kleemann, Catal. Today 59 (2000) 335–345.
[24] A. Ivanova, E. Slavinskaya, V. Mokrinskii, I. Polukhina, S. Tsybulya, I. Prosvirin, V. Bukhtiyarov, V. Rogov, V. Zaikovskii, A. Noskov, J. Catal. 221 (2004) 213–224.
[25] F. Kapteijn, L. Singoredjo, M. van Driel, A. Andreïni, J.A. Moulijn, G. Ramis, G. Busca, J. Catal. 150 (1994) 105–116.
[26] M. Anstrom, N. Topsøe, J.A. Dumesic, J. Catal. 213 (2003) 115–125.
[27] G. Marbán, T. Valdés-Solís, A.B. Fuertes, J. Catal. 226 (2004) 138–155.
[28] F.J.J.G. Janssen, F.M.G. van den Kerkhof, H. Bosch, J.R.H. Ross, J. Phys. Chem. 91 (1987) 5921–5927.
[29] F.J.J.G. Janssen, F.M.G. van den Kerkhof, H. Bosch, J.R.H. Ross, J. Phys. Chem. 91 (1987) 6633–6638.